View metadata, citation and similar papers at core.ac.uk

brought to you by CORE

provided by Publications at Bielefeld University

In situ scanning-tunneling-microscopy studies of current driven mass transport in Ag

L. E. Levine,[a] G. Reiss,[b] and D. A. Smith[c]
IBM Research Division, T. J. Watson Research Center, Yorktown Heights, New York 10598

(Received 22 December 1992; accepted for publication 11 June 1993)

We present the results of an ultrahigh vacuum (UHV) scanning-tunneling-microscopy study of large scale mass transport in current carrying metal films. Scans were taken *in situ* on a current carrying 2100-Å-thick Ag film with current densities ranging from 5.0×10^4 A/cm^2 up to 3.2×10^5 A/cm^2, at which point the sample failed due to a runaway thermal fusing mechanism. Axial UHV inchworms allowed us to obtain data from the same 2-μm-square region of the sample throughout the experiment in spite of large temperature-induced drifts. Calculations of the driving forces demonstrate that the electromigration driving force was dominant for this current range. Significant topographical changes were observed including current aligned grain growth, current induced faceting, and complex mass flow divergences. A model that explains the observed divergences is presented. It is based upon diffusion in the presence of local inhomogeneities of the electric field.

INTRODUCTION

The study of mass transport in current carrying lines and films is a topic of great interest both for its practical importance as a failure mechanism in circuit elements and for improving our basic knowledge of this complex phenomenon. This mass transport is basically a solid state diffusion mechanism driven by electrical, thermal, and mechanical forces; each of these forces, in turn, has a number of components and depends critically upon the specifics of the experiment. For experiments performed near room temperature on uncapped samples, the electrical driving force often dominates; the resulting mass flow is then called electromigration. The various diffusion pathways include surface, grain boundary, and bulk diffusion. Many other factors such as the sizes and orientations of the grains, the dimensions of the investigated structures, the role of second phase grain boundary precipitates on solute diffusion, and the presence of inhomogeneous electric fields can significantly affect the mass transport process in real materials. For recent reviews of these related problems see, for example, the discussions given by Ho and Kwok[1] or Scorzoni *et al.*[2]

Since all of these phenomena are operative at very small length scales, *in situ* high-resolution microscopy is clearly important for understanding the basic mass transport mechanisms involved. As we have discussed in previous publications,[3,4] the scanning tunneling microscope is particularly well suited for this task because of its nondestructive nature, its extremely high resolution ($\approx$atomic), and its ability to provide quantitative height profiles of the sample.

As previously reported, we have constructed an ultrahigh vacuum (UHV) scanning-tunneling-microscope (STM) system capable of studying annealing and electromigration processes *in situ* on heated and/or current carrying thin films.[3,4] The system uses an ac feedback (potentiometric design) that overcomes the problem of decoupling the STM electronics from the dc voltage drop over a current carrying sample. UHV inchworms on all three axes provide coarse motion to compensate for drifts during sample heating.

We recently published the first *in situ* UHV STM study of electromigration in thin metal films.[4] In this publication we described the early stage electromigration changes observed on a 2100 Å Ag film. We define the early stage electromigration regime as the time and current density range in which the sample resistance remains constant to within 1% of the initial value ($\Delta R/R_0<1\%$). These changes included the growth of small nodules (<30 Å in height) at grain boundary triple points, current induced grain boundary grooving, and a grain growth mechanism that strongly resembles classical thermally induced grain growth. The changes took place at very small length scales and could not have been resolved using any other available microscopic technique. In this paper, we present the results of an *in situ* topographic STM study of late stage electromigration in an Ag film. We define the late stage electromigration regime as the time and current density range from the point where the sample resistance has changed by more than 1% of its initial value, up to sample destruction. The topographical changes observed in the film are fundamentally different from those observed during early stage electromigration. These late stage changes involve significant mass transport and include current induced faceting, surface grain growth, agglomeration, and a previously unreported growth mechanism probably driven by inhomogeneous electric fields. We are in communication with another research group that is using an in-air STM/atomic force microscope for studying electromigration in Au lines.[5]

[a]Present address: Department of Physics, Washington University, St. Louis, MO 63130.
[b]Present address: IFW Dresden, Helmholtz Str., Dresden 0-8027, Germany.
[c]Present address: Dept. Mater. Sci. Eng., Stevens Institute of Technology, Castle Point on the Hudson, Hoboken, NJ 07030.

 0021-8979/93/74(9)/5476/7/$6.00 © 1993 American Institute of Physics

Downloaded 22 Oct 2008 to 129.70.165.221. Redistribution subject to AIP license or copyright; see http://jap.aip.org/jap/copyright.jsp

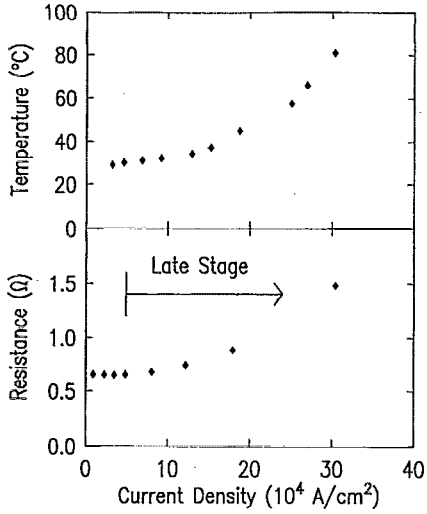

FIG. 1. Temperature and resistance calibration curves for our 2100 Å Ag film samples.

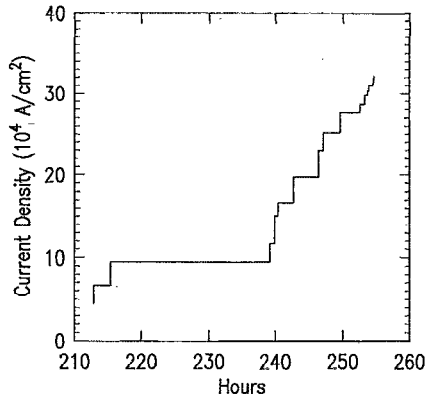

FIG. 2. Applied dc current density as a function of time for our second electromigration experiment on Ag films.

EXPERIMENT

Our Ag films were produced by evaporation onto room temperature mica substrates at a rate of 2 Å/s with a base pressure of 9×10^{-8} Torr. The film thickness was 2100 Å. Auger depth profiling showed significant oxygen contamination at the surface that decreased to $\approx$ monolayer after three days in UHV. Other significant surface contaminants included Cl ($\sim$10%), C ($\approx$10%), and S (2%–3%). Most of this surface contamination was swept away by surface diffusion upon application of a small electric current (1.4×10^4 A/cm^2) for a period of several days, as reported in our paper on early stage electromigration.[4]

Sample resistance and temperature as a function of current density were measured in a separate vacuum chamber for multiple identical samples. Sample current was increased slowly for these measurements over a period of many days until sample failure. Post-failure scanning electron microscopy (SEM) studies were carried out on all electromigration samples and showed the same thermal-runaway failure mechanism. The film temperature was measured using a small mass thermocouple in contact with the film surface. Resistance was measured using a quasi four point probe arrangement. All resistance and temperature measurements were consistent. Representative curves for the late stage electromigration regime are shown in Fig. 1.

As-deposited Ag films were examined in a Philips 430 TEM with a beam voltage of 300 kV. Microdiffraction, selected area diffraction, and real space imaging were used to determine grain sizes and orientations.[4] Results show the film to be weakly (111) textured. The observed grain size distributions are consistent with the idea that the granular structure apparent in the STM corresponds to actual grains delineated by small scale grain boundary grooving. This topic will be discussed in greater detail in a separate publication.[6]

The Ag films examined in the UHV STM measured 5 mm between the electrical contacts and were 1.5 mm wide. The samples were studied at a base pressure of 1×10^{-10} Torr. Two separate samples were studied using the same experimental procedure. The first sample was used primarily as a test case to prepare for a more in-depth study on the second sample. The results from both experiments were consistent and we will primarily concentrate on results from the second electromigration sample. During the *in situ* electromigration studies, our procedure was to increase the dc sample current by a few mA and take repeated scans of one general area for several hours. Current was applied using a constant current source. Scan sizes ranged from 2.0 down to 0.1 μm square. If no significant changes were observed, the sample current was again increased. During the second run, this procedure continued for 256 h until the sample failed at a current density of 3.2×10^5 A/cm^2. For most of this time, $\Delta R/R_0$ remained constant to within $<1\%$. The results of this early stage electromigration study have already been published.[4] Figure 2 shows the dc sample current as a function of time for the late electromigration stage of our second run. During this period, 162 scans of the sample were taken. We used the UHV inchworms to compensate for sample drift and stayed approximately centered over the same 2-μm-square area of the sample throughout the experiment.

In order to separate the effects of annealing and current flow, we also completed an *in situ* STM study on an indirectly heated Ag film. A maximum temperature of 140 °C was reached after 391 h. None of the structural changes reported in this article were observed in the indirectly heated sample.

All of the STM images displayed in this article, except for Fig. 5, were obtained from 750-nm-square topographic scans composed of 256×256 data points. A plane was subtracted from the data and no other image processing algorithms were used. Figure 5 was taken from a 2000-nm-square topographic scan. The ac bias voltage was 300 mV and the ac tunneling current was 10 nA. The tunneling tip was produced from a 0.5 mm electrochemically etched tungsten wire. SEM studies of identically prepared tips showed them to have a radius of $\leqslant$50 nm.

Downloaded 22 Oct 2008 to 129.70.165.221. Redistribution subject to AIP license or copyright; see http://jap.aip.org/jap/copyright.jsp

DRIVING FORCES AND MASS TRANSPORT

The primary driving forces that can bias atomic motion in metal films are electrical, thermal, and mechanical in nature. Electromigration results from the electrical driving force and is usually described by the expression:

$$\mathbf{F}_E = Z^* e \mathbf{E} = Z^* e \rho \mathbf{j}, \tag{1}$$

where $\mathbf{E}$ is the electrostatic field, ρ is the resistivity of the metal, $\mathbf{j}$ is the local current, and Z^* is the effective charge number.[2] Using the room temperature resistivity of Ag and the approximate value[1] of $Z^* = -8$ gives:

$$\mathbf{F}_E = \mathbf{j}(1.3 \times 10^{-3})(\text{eV/m}), \tag{2}$$

where $\mathbf{j}$ is in units of A/cm^2. Since the maximum current density reached during this experiment was 3.2×10^5 A/cm^2, the maximum $\mathbf{F}_E$ was thus 416 eV/m. The negative sign on the effective charge indicates that the electron wind force dominates and so we expect metal motion in the direction of the electron particle flux.

As shown in Fig. 1, Joule heating during this experiment raised the Ag film to a maximum temperature of 90 °C. We can, therefore, set an upper bound for the temperature gradient of 26 °C/mm, as determined by our sample geometry. The driving force resulting from thermal gradients is described by the equation:

$$\mathbf{F}_T = -Q^* \frac{\nabla T}{T},$$

where Q^* is the heat of transport and equals the energy flow per unit mass transported minus the intrinsic heat of solution.[7] Experimental measurements for Q^* in the literature are inconsistent for most metals. Using an extreme upper bound estimate of 0.5 eV for Q^* (Q^* for Al is 0.03 eV) gives 32 eV/m as an upper bound for our maximum $\mathbf{F}_T$. Since $\mathbf{F}_E \propto \mathbf{j}$, and $\mathbf{T}$ increases faster than linearly with $\mathbf{j}$ as shown in Fig. 1, we conclude that $\mathbf{F}_E$ is dominant over $\mathbf{F}_T$ throughout the entire current range of this experiment.

The three major components of the mechanical induced driving force are the intrinsic process-induced stress field, the stress field produced by differing thermal expansions of the film and substrate during Joule heating, and the stress gradients induced by electromigration. The samples used in this experiment are the same samples previously used for our study of early stage electromigration in Ag. In this study, we examined the role of mechanical driving forces for current densities less than 5.0×10^4 A/cm^2 at temperatures near room temperature and we determined that these mechanical driving forces were small when compared with the electromigration driving force.[4] Although the current densities and temperatures were much higher during our experiment on late stage electromigration, the previous analysis remains valid for these new conditions. This analysis, however, does not address the problem of highly localized gradients in the region of structural changes, which could still play a significant role in the evolution of such structures.

We have shown that electromigration is the dominant driving force for mass transport in our Ag films. The diffusion mechanisms include lattice (bulk), grain boundary, and surface diffusion. An expression for the mass flux $\mathbf{J}_a$ for the diffusion mechanism a is

$$\mathbf{J}_a = \mathbf{j} \frac{N_a Z^* e \rho}{kT} D_{0a} \exp\left(\frac{-\mathbf{E}_a}{kT}\right), \tag{3}$$

where N_a is the mobile element atomic density, D_{0a} is a temperature-independent preexponential term for the given mechanism, and $\mathbf{E}_a$ is the activation energy for the mechanism.

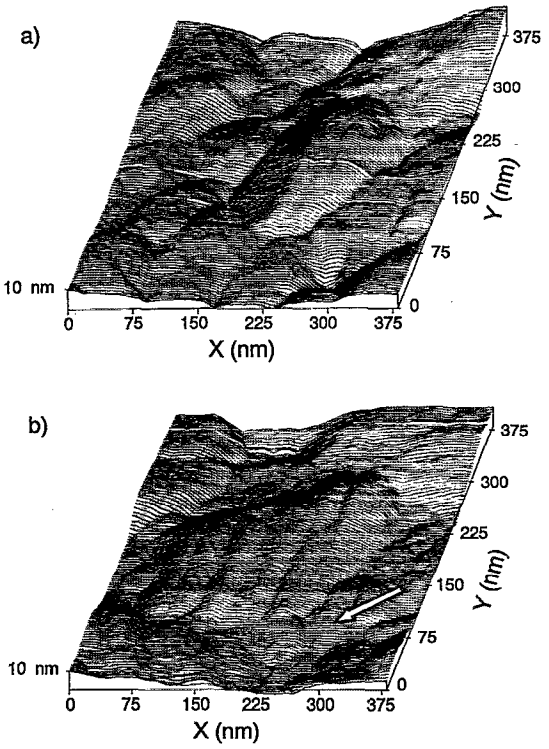

FIG. 3. Topographic STM scans of the same faceted Ag grain taken at (a) 73.3 h, 2.1×10^4 A/cm^2 and (b) 218.0 h, 9.5×10^4 A/cm^2. The surface of the grain has grown in the direction of the electron flux and additional faceting has taken place. The arrow points in the direction of the electron flux.

RESULTS

The first major topographical change that occurred in our Ag sample is shown in Fig. 3. The scan in Fig. 3(a) was taken 73.3 h into the experiment at a current density of 2.1×10^4 A/cm^2 and a temperature of 28 °C. The topography of the central grain is unchanged from earlier as-deposited scans. This grain shows a clear faceting structure with a large, almost atomically flat area and distinct facets on the right side. Conventional thermal faceting theory suggests that a faceted surface consists of a set of low-index (low surface energy) planes and a set of more complex planes making a contact angle θ with the low-index planes.[8] Previous measurements on thermally faceted Ag crystals indicate that, for this metal, the low-index planes are either (100) or (111).[9]

Figure 3(b) shows a scan of the same grain taken 218 h into the experiment at a current density of 9.5×10^4

Downloaded 22 Oct 2008 to 129.70.165.221. Redistribution subject to AIP license or copyright; see http://jap.aip.org/jap/copyright.jsp

A/cm^2 and a temperature of 33 °C. At this stage of the experiment, $\Delta R/R_0 \approx 7\%$. The central grain has grown significantly in the direction of the electron flux. Similar growth behavior was observed on other grains within the 2-μm-square maximum scan area. In all cases, growth was in the direction of the electron flux. The parallel facets on the grain shown in Fig. 3 demonstrate that the enlarged grain grew from the original smaller grain and maintained the same crystallographic orientation. The facets have a height range of 20–30 Å, an average contact angle of 16°, and an average spacing of 30 Å.

The pronounced faceting previously described was not observed in the indirectly heated sample we examined. This demonstrates that the facet growth was current induced and was most likely caused by electromigration. Thermal and current induced faceting have been previously studied[8–10] and it has been shown that such faceting is usually caused by either evaporation of material from selected crystal planes or by minimization of surface energy by atom transport to lower energy configurations. This atom transport can take place by either evaporation/condensation or by surface diffusion. Evaporation from selected crystal planes and evaporation/condensation as a mass transport mechanism are both ruled out by the low temperature of our sample, thus leaving surface energy minimization by current driven surface diffusion as the most probable mechanism for the observed facet growth. This suggestion is supported by the observed growth direction of the grain shown in Fig. 3. Since layer nucleation would be energetically unfavorable on the large, low-energy flat surface shown in Fig. 3(a), diffusing adatoms would be driven in the direction of the electron flux to the higher energy edge of the plane. Nucleation of additional facets would be more energetically favorable at this location. Continued surface diffusion in this direction would thus result in a series of facets with a net growth in the direction of the electron flux. The small raised feature at the far left edge of the grain in Fig. 3(b) was not present in Fig. 3(a) and could be a facet nucleation site.

Since topographical STM scans only provide surface information, we cannot conclusively determine whether the observed grain growth continues into the bulk or if the growth is primarily restricted to the surface of the sample. Earlier experiments have shown that surface diffusion is the dominant mass transport mechanism in Ag for the temperature range of this experiment.[11] The faceting described previously confirms that surface diffusion is significant in our sample at this current density. Although subsurface grain growth would be energetically favored by reducing the grain-boundary area, such growth would require significant atomic motion within the grain boundaries and is probably kinetically limited.

Figure 4 shows the same grain at 243.6 h, 2.0×0^5 A/cm^2, and 45 °C. At this stage, $\Delta R/R_0$ has increased to 49%. The orientation of Fig. 4 is identical to the orientations of Figs. 3(a) and 3(b) so the electron flow is primarily right to left. Comparison with Fig. 3(b) shows that a large redistribution of material has taken place, resulting in a pronounced elevation of the grain with respect to its base.

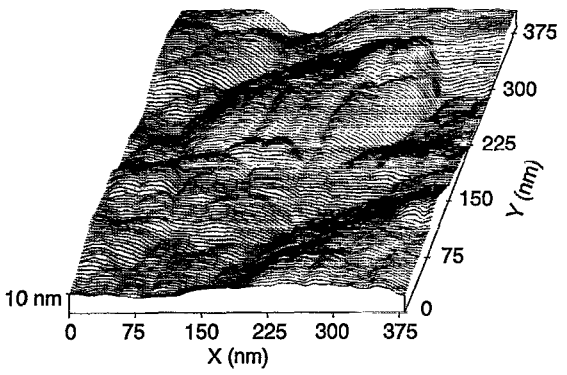

FIG. 4. Topographic STM scan of the same grain shown in Fig. 3, but taken at 243.6 h, 2.0×10^5 A/cm^2, and 45 °C. A divergence of the mass flow has resulted in a significant redistribution of material.

This elevation is significantly larger on the upstream side of the grain. At this location, the height of the grain is approximately 200 Å. Further evidence of this massive redistribution of material can be seen in the wide grooves surrounding much of the central grain. Similar morphology changes occurred throughout the entire scanned area of the sample. Since mass is preferentially accumulating at the leading edge of the grain in Fig. 4, this location is, by definition, an area of mass flux divergence.

To understand the reasons for this divergence, we must examine the driving forces on a migrating atom when it encounters a raised area of height h on a sample of uniform thickness t. For $h \ll t$, we can use the approximation of a uniform current flow through the sample. The current density through the raised area of the sample must, therefore, decrease by the ratio h/t due to the difference in cross-sectional area. As demonstrated previously, the dominant driving force in this experiment is the electromigration force which is proportional to the current density as shown in Eqs. (1) and (2). For the grain shown in Fig. 5, we can, therefore, estimate the percentage change in the driving force to be $\approx$200 Å/2000 Å$=10\%$. As shown in Eq. (3), the expected mass flux is also proportional to the current density. The units for the mass flux $\mathbf{J}$ are atoms/m^2/s. The number of atoms/s moving through the bulk must therefore equal $\mathbf{J}_b$ times the cross-sectional area. The increase in the cross-sectional area of the raised portion of the film therefore exactly cancels out the decrease in $\mathbf{J}_b$ leaving the net mass flow unchanged. This is true for any nonsurface diffusion mechanism, including both bulk and grain boundary diffusion. For surface diffusion, however, the decrease in the driving force is mostly uncompensated, resulting in a divergence of the mass flow. This suggested mechanism also explains the observed fact that all of the raised features within the maximum scan area are growing at this stage, and the higher features are growing more rapidly than the lower ones.

Figure 5 shows additional raised features on the sample at a later time in the experiment. No small-area scans were taken of these features so this figure is a selected area from a larger image. The scan was taken at 249.9 h,

Downloaded 22 Oct 2008 to 129.70.165.221. Redistribution subject to AIP license or copyright; see http://jap.aip.org/jap/copyright.jsp

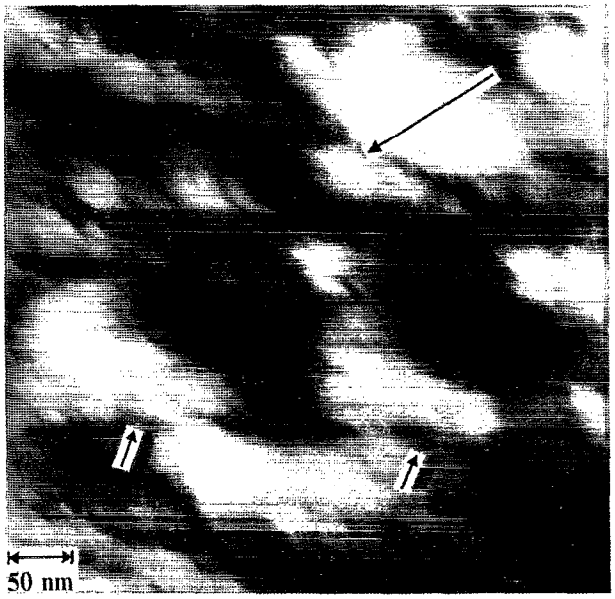

FIG. 5. Gray-scale image of a topographic STM scan with a height scale of 200 Å (black-white). The two indicated crescent shapes with central depressions are probably caused by electromigration driven surface diffusion in the presence of local, inhomogeneous electric fields. The large arrow points in the direction of the electron flux.

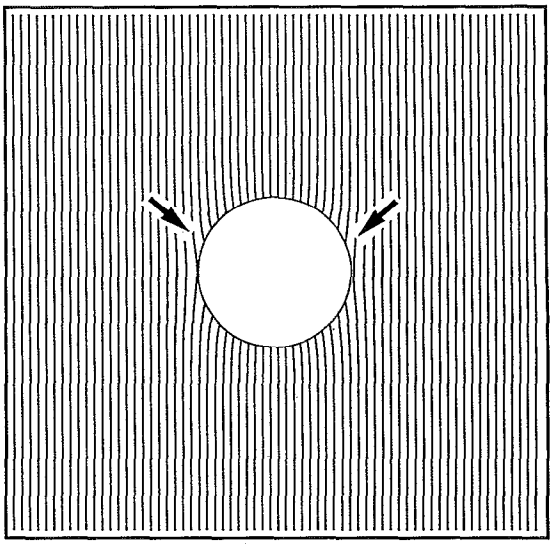

FIG. 6. Calculated lines of current flow on the surface of a conductive plane in the vicinity of a raised projection. The arrows point to two regions where mass accumulation is expected.

2.7×10^5 A/cm^2, and 66 °C. At this stage of the experiment, $\Delta R/R_0$ has increased to approximately 96%. The height scale for the image is 200 Å (black-white) and the arrow points in the direction of the electron flux. The raised features have developed into crescent shapes with the open sections pointed toward the electron source. Depressions are clearly visible immediately upstream of the crescents.

To understand this phenomenon empirically, we must re-examine the current flow model for the case where h is not much smaller than t. In this case, the approximation of a uniform current flow through the sample becomes invalid. Since the electrical resistance through a conductor is proportional to the cross-sectional area, the total current flowing through a raised area of the sample will be increased. It is therefore clear that the electric field lines must "bunch" in the vicinity of a raised area and spread apart in the vicinity of a depressed region. Since this additional change in the electric field is not compensated for by changes in the cross-sectional area, mass divergences through bulk and grain-boundary diffusion again become possible. For our experiment, however, it is probable that surface diffusion still dominates this process.

For the case of a raised area on a uniform film, the regions of the sample with the highest current density would be directly in front of and directly behind the raised area; the region with the lowest current density would be within the raised area. Figure 6 shows the calculated lines of current flow on the surface of a 2000-Å-thick uniform conductive film with a 200-Å-high projection. The electric potential, and thus the electric field within the conductor, was calculated by using a finite element analysis technique to solve the three dimensional Laplace equation. The local currents were then calculated from the equation $\mathbf{j}=\sigma\mathbf{E}$. The apparent symmetry is split by the direction of the electron flux. A diffusing atom would therefore experience an increasing current density on the upstream side of the raised area and a decreasing current density on the downstream side. Let us examine the net mass flux in a region of increasing current density. At any given point, there is a flux of material arriving from upstream and a flux of material leaving downstream. Since $\mathbf{J}\propto\mathbf{j}$ by Eq. (3), the mass flux arriving from upstream must, therefore, be less than the material leaving downstream, resulting in a net depletion. This process is reversed within a region of decreasing current density resulting in a net mass accumulation. We would therefore expect increased mass loss directly in front of the raised area resulting in the depressions observed in Fig. 5. Following a similar line of reasoning, we would also expect a net mass accumulation on the upstream sides of the raised area as marked by the arrows in Fig. 6. The resulting mass configuration is the crescent/hole structure observed in Fig. 5.

Continued evolution of the crescent/hole structure is difficult to predict without detailed computer modeling of the entire development process. Calculation of current and heat flow distributions for each step should follow the finite-element analysis techniques used by Kwok *et al.* in their calculations on multilevel structures.[12] Work on these calculations is in progress.

Figure 7 shows the next morphology change we observed in our samples. This scan was taken at 251.2 h, 2.7×10^5 A/cm^2, and 66 °C. The height scale is 300 Å (black-white). The ring shapes were formed by a buildup of material upstream of the crescent/hole structures. In terms of the model we have presented, this buildup could have been caused by a decreasing current density upstream

Downloaded 22 Oct 2008 to 129.70.165.221. Redistribution subject to AIP license or copyright; see http://jap.aip.org/jap/copyright.jsp

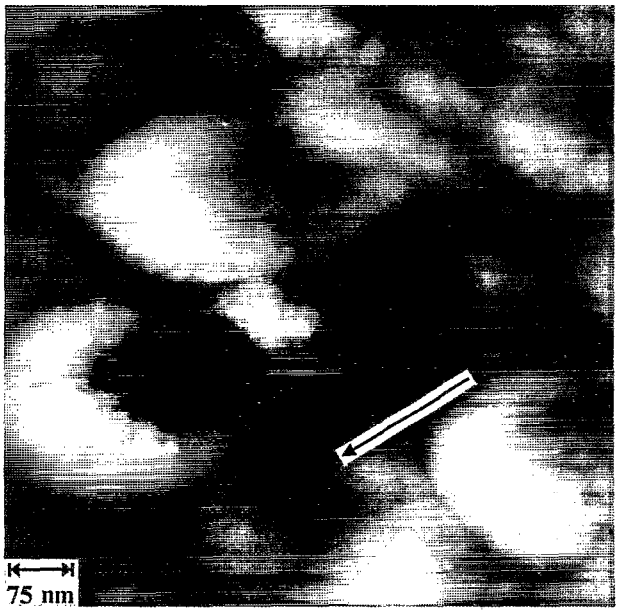

FIG. 7. Early ring structures that evolved from crescent shapes similar to those shown in Fig. 5. The height scale is 300 Å (black-white) and the arrow points in the direction of the electron flux.

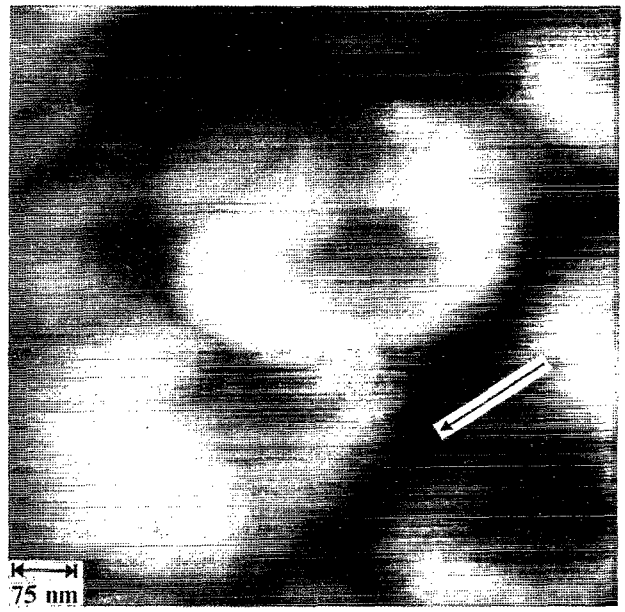

FIG. 8. Double-ring structure aligned with the direction of the electron flux as shown by the arrow. The height scale for the image is 530 Å (black-white).

of the crescents. Such a current flow pattern seems reasonable since the forward arms of the crescent would have a lower resistance than the central depressed region.

We have described empirically how electromigration driven diffusion in the presence of local, inhomogeneous electric fields could produce the raised area→crescent/hole→ring sequence observed in this experiment and shown in Figs. 3–7. By this same process, we can consider the leading edges of these rings to be raised areas that should produce additional rings, roughly aligned with the current flow. Such linked-ring features were seen frequently over the scanned region of the sample. A representative double-ring structure is shown in Fig. 8. This scan was taken at 252.3 h, 2.8×10^5 A/cm^2, and 71 °C. At this stage, $\Delta R/R_0$ has increased to $\approx$104%. Triple-ring structures that are aligned with the current flow were also observed.

All of the crescents, depressions, and rings have almost identical dimensions at the same stages of their evolution, completely independent of the original underlying grain structure. Any mechanism proposed for this process must therefore be mostly independent of such microstructural details. The diffusion mechanism we have proposed satisfies this requirement. Calculation of the expected length scales of these features involves many factors and work on computer simulations of the ring evolution process is in progress.

Once formed, the ring structures retain their same general shape but continue to accumulate mass by growing in both width and height. Rings were observed with widths of $\approx$4000 Å and heights of $\approx$1000 Å. Such large mass accumulations on a 2100-Å-thick film require significant depletion of the material in the intervening low regions, resulting in higher sample resistance and inhomogeneous Joule heating.

Sample failure occurred through a runaway thermal fusing mechanism at 254.7 h at a current density of 3.2×10^5 A/cm^2. Figure 9 shows a 0.75-μm square scan of the sample immediately prior to this event. The grains in this image evolved from the large rings. The straight grain boundaries, the well-defined angles at the triple points, and the lack of small surface detail suggest that a different growth mechanism dominates at this late stage; this mechanism strongly resembles classical thermally induced grain growth. Temperature measurements during these final stages are unreliable due to the rapidity of the sample breakdown process. Post-failure SEM studies on the sample show evidence of dewetting and local melting in the breakdown region of the sample.

CONCLUSIONS

We have presented the results of an *in situ* UHV STM study of current driven mass transport on an Ag film. Current density in the sample was increased from 5.0×10^4 to 3.2×10^5 A/cm^2 over a period of 42 h. During this period, sample temperature increased from 32 to 90 °C and the sample resistance increased from $\Delta R/R_0=1\%$ up to sample destruction. A total of 162 scans of the sample were taken.

Calculations of the electrical, thermal, and mechanical driving forces for the sample showed that the electromigration driving force was dominant for the entire current range of the experiment.

The first major topographical changes that were observed in the sample were current aligned surface grain growth and current induced faceting. These changes oc-

Downloaded 22 Oct 2008 to 129.70.165.221. Redistribution subject to AIP license or copyright; see http://jap.aip.org/jap/copyright.jsp

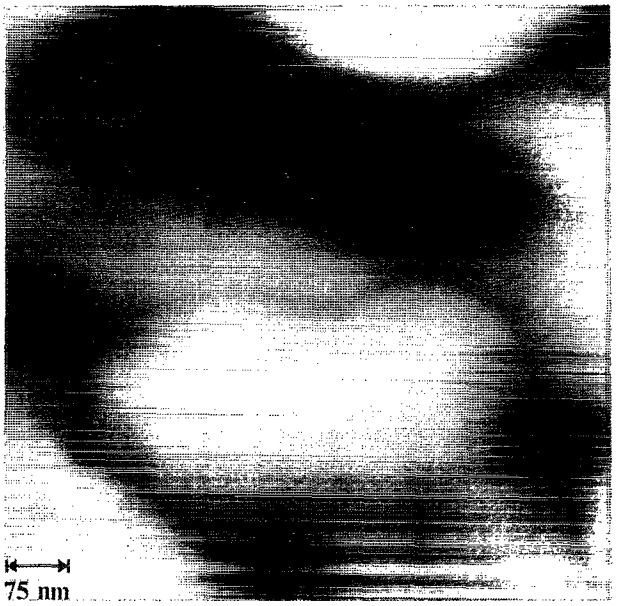

FIG. 9. STM scan showing sample morphology immediately before the sample died through a runaway thermal fusing mechanism. The grains developed from large ring structures. The height scale for the image is 1100 Å (black-white).

curred at a current density of 9.5×10^4 A/cm^2 and were probably caused by electromigration driven surface diffusion. These features had a maximum height of just 30 Å and could not have been resolved using any other presently available technique. Mass flow divergences were detected at a current density of 2.0×10^5 A/cm^2. These divergences appeared as current aligned height increases of already protruding surface features. An empirical model based on surface diffusion and inhomogeneous electric fields was presented to explain these results. At a current density of 2.7×10^5 A/cm^2, these mass divergences evolved into crescent shapes with upstream depressions. These crescent shapes were also aligned with the current flow. The crescents later changed into complete rings at the same current density. Finally, linked-ring systems developed that were roughly aligned with the current flow. The rings continued to accumulate mass by growing in both width and height. Rings were observed with widths of $\approx$4000 Å and heights of $\approx$1000 Å. An extension of the inhomogeneous electric field model was used to explain this entire sequence of changes. The concentration of mass in the ring structures resulted in a runaway heating effect. Immediately prior to final sample destruction, the sample transformed into a lower energy grain structure through a mechanism that was probably thermally induced grain growth.

The mass divergences observed in this experiment demonstrate clearly that inhomogeneous electric fields can play an important role in electromigration phenomena. Such effects are not restricted to surface diffusion and could contribute significantly to the local stress gradients in capped lines and studs.

Whenever a new, powerful experimental technique is developed for examining a complex physical process, the result is a rich hunting ground for both the experimentalist and the theorist. In this article, we presented the first *in situ* UHV STM observations of large scale mass transport in current carrying metal films. Many of the observed topographical changes, such as the surface grain growth and current induced faceting, could not have been resolved using any other presently available experimental technique. The later stages of the ring-structure evolution could have been seen using SEM but the early stages of their development would have been missed without a UHV STM. It was these early stages that provided evidence for the inhomogeneous electric field model presented in this article.

[1] P. S. Ho and T. Kwok, Rep. Prog. Phys. **52**, 301 (1989).
[2] A. Scorzoni, B. Neri, C. Caprile, and F. Fantini, Mater. Sci. Rep. **7**, 143 (1991).
[3] G. Reiss, L. E. Levine, and D. A. Smith, J. Vac. Sci. Technol. B **11**, 108 (1993).
[4] L. E. Levine, G. Reiss, and D. A. Smith, Phys. Rev. B **48**, 858 (1993).
[5] M. Paniccia, P. Flinn, and R. Reifenberger, J. Appl. Phys. **73**, 8189 (1993).
[6] G. Reiss and L. E. Levine (unpublished).
[7] H. B. Huntington, Thin Solid Films **25**, 265 (1975).
[8] A. J. W. Moore, in *Metal Surfaces: Structure, Energetics and Kinetics* (American Society for Metals, Metals Park, OH, 1962), p. 155.
[9] A. J. W. Moore, Acta Metall. **6**, 293 (1958).
[10] P. Adam, Z. Naturforsch. Teil. A **26**, 40 (1971).
[11] R. E. Hummel and H. J. Geier, Thin Solid Films **25**, 335 (1975).
[12] T. Kwok, T. Nguyen, P. Ho, and S. Yip, *Proceedings of the 4th IEEE VLSI Multilevel Interconnection Conference* (IEEE, New York, 1987), p. 252.

Downloaded 22 Oct 2008 to 129.70.165.221. Redistribution subject to AIP license or copyright; see http://jap.aip.org/jap/copyright.jsp